

NJC

Accepted Manuscript



This is an *Accepted Manuscript*, which has been through the Royal Society of Chemistry peer review process and has been accepted for publication.

Accepted Manuscripts are published online shortly after acceptance, before technical editing, formatting and proof reading. Using this free service, authors can make their results available to the community, in citable form, before we publish the edited article. We will replace this *Accepted Manuscript* with the edited and formatted *Advance Article* as soon as it is available.

You can find more information about *Accepted Manuscripts* in the [Information for Authors](#).

Please note that technical editing may introduce minor changes to the text and/or graphics, which may alter content. The journal's standard [Terms & Conditions](#) and the [Ethical guidelines](#) still apply. In no event shall the Royal Society of Chemistry be held responsible for any errors or omissions in this *Accepted Manuscript* or any consequences arising from the use of any information it contains.



Journal Name

ARTICLE

The syntheses, structural and azo-hydrazone tautomeric studies of three triazole/tetrazole azo dyes

Jiawei Cai, Zhixin Li, Yanxuan Qiu, Zhijian OuYang, Wenning Lin, Liu Yang, Weijin Feng, Xinwei Yu and Wen Dong*

Received 00th January 20xx,
Accepted 00th January 20xx

DOI: 10.1039/x0xx00000x

www.rsc.org/

Three heterocyclic azo dyes of azotriazolyl-2,7-dihydroxynaphthalene (H₃AD), azotetrazolyl-2-naphthol (H₂ATN) and azotetrazolyl-2,7-dihydroxynaphthalene (H₃ATD) have been synthesized and characterized by IR, Raman spectra, ¹H, ¹³C NMR and X-ray single-crystal diffraction techniques and their azo-hydrazone tautomerism have been achieved by pH control and coordination-coupled proton transfer. UV-vis spectra have been used to monitor the pH-titration and metal-ion complex experiments for three solutions of H₃AD, H₂ATN and H₃ATD and the analysis of their spectra data have provided a clear proof that the hydrazone form is the dominant tautomer in acidic and neutral solutions, while the azo form is the dominant one in alkaline solution. Crystallographic data demonstrate that the neutral dyes are hydrazone former but are changed to azo tautomers when they coordinate to metal ions. The time-dependent density functional theory (TD-DFT) calculations are used to demonstrate the UV-vis spectroscopic properties.

1. Introduction

Aromatic azo compounds have found wide application as dyes in optical and color-changing materials such as sunglasses, textiles, paints, cosmetics, and food additives.^{1–6} In contrast to azobenzenes, heterocyclic azo compounds are less well investigated, although they have shown brilliant color and chromophoric strength.^{6–9} Azo dyes account for 60–70% of all dyes produced in the world.^{3,4} In azo compounds, the azo group (–N=N–) usually undergo reversible *trans*–*cis* photoisomerization that can also be exploited in the design of photoswitches, molecular motors, etc.^{10–13} and even in the development of potential photothermal sensitizers in the photodynamic therapy of some forms of cancer and other diseases.^{14,15} The aromatic azo compounds having hydroxyl groups in ortho or para positions may give rise to two distinct isomers: azo or hydrazone tautomers, which may coexist under certain experimental conditions.³ The investigation of interconversion between the azo and hydrazone isomers are still currently hot interesting from structures to properties although azo to hydrazone tautomerism have been reported by pH control and coordination-coupled proton transfer for several azo dyes.^{16–21} Up to now, several techniques such as IR,

Raman, NMR spectra and X-ray single-crystal diffraction method have been employed to elucidate the structures of numerous azo compounds, the precise assignments of the spectroscopic signs of azo–enol or hydrazone–keto tautomers are still incomplete in the medium.⁴ X-ray single crystal diffraction has been proved to be the most powerful tool to characterize various azo compounds by analyzing the data of bond lengths and angles, dihedral and torsion angles, and supramolecular interactions in solid state and the structural information are in relation with optical properties as well as with technical properties of azo dyes and pigments.²² On the other hand, the ¹H NMR spectrum has been employed to demonstrate the azo–hydrazone tautomerism by analyzing the chemical shifts of the hydrazone proton and the ¹³C NMR spectrum has been employed to demonstrate the azo–hydrazone tautomerism by analyzing the changing chemical shifts of carbon atoms of azo–enol and hydrazone–keto isomers.^{5,23} Detailed knowledge on the structures and photochemical behavior of aromatic heterocyclic azo compounds is crucial for understanding their reactivity and applications.³ In our previous work, several aromatic heterocyclic azo compounds and their azo–metal complexes have been reported.^{24–27} Here, we report the syntheses, structures and spectroscopic properties of three heterocyclic azo dyes of H₃AD, H₂ATN and H₃ATD and their azo–hydrazone tautomerism have been observed and demonstrated.

2. Experimental

2.1. Materials and physical measurements

All the commercial reagents and solvents were used without further purification unless otherwise stated. ¹H and ¹³C NMR

School of Chemistry and Chemical Engineering, Guangzhou Key Laboratory for Environmentally Functional Materials and Technology, Guangzhou University, Guangzhou, 510006, China, E-mail: dw320@aliyun.com; Tel: +86-20-31876185; Fax: +86-20-39366902

*Electronic Supplementary Information (ESI) available: Crystallographic data in CIF format, crystal data and data collection parameters, mass spectrum and atomic labeling diagram for ring-closure product of H₃AD, UV-vis spectra of H₃AD, H₂ATN and H₃ATD, the calculated electronic spectra of H₃AD, H₂ATN and H₃ATD using TD-DFT at mPW1PW91/6–311++G(d,p) level and CAM-B3LYP/6–311++G(d,p) level. See DOI: 10.1039/x0xx00000x

spectra were recorded on a 500 MHz Digital NMR Spectrometer (AV III, Ascend 500 HD). UV–vis absorption spectra of H₃AD, H₂ATN and H₃ATD in aqueous solution were collected on U–2550 Ultraviolet–Visible Spectrophotometer. IR spectra were recorded as pressed KBr pellets on a Bruker Tensor 27 spectrophotometer with an average of 64 scans. Raman spectra were obtained from the solid phase, using Bruker VERTEX 70 Raman instrument with excitation at 1064 nm from a ND:YVO₄ laser, power in 200 mW with an average of 60 scans. Elemental analyses were carried out using a Perkin–Elmer analyzer model 240.

2.2. X-ray crystallography and data collection

The crystals were filtered from the solution and immediately coated with hydrocarbon oil on the microscope slide. Suitable crystals were mounted on glass fibers with silicone grease and placed in a Bruker Smart APEX(II) area detector using graphite monochromated Mo–K α radiation ($\lambda = 0.71073 \text{ \AA}$) at 296(2) K. The structures were solved by direct methods, and all non-hydrogen atoms were refined anisotropically by least-squares on F^2 using the SHELXL-97 or SHELXL-2014 programs. Hydrogen atoms were located from difference maps and refined with isotropic temperature factors. Table S1 gives the crystal data of H₂ATN, [Ni(H₂AD)₂] \cdot 4H₂O and the ring-closure product of H₃AD (ESI[†]). The final consistency factors of $R = 0.0394$ ($R_w = 0.0917$) for H₂ATN, $R = 0.0505$ ($R_w = 0.1083$) for the ring-closure product of H₃AD and $R = 0.0686$ ($R_w = 0.2009$) for [Ni(H₂AD)₂] \cdot 4H₂O were given. The bond lengths and angles for the three compounds are listed in Table 1.

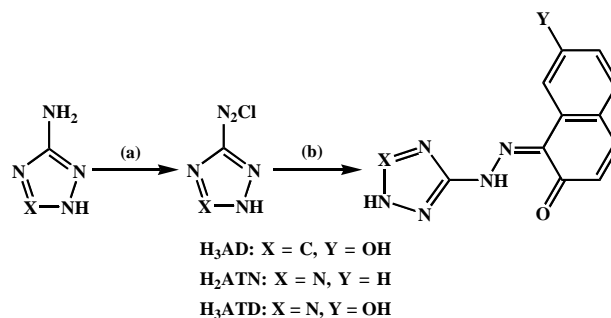
2.3. Theoretical calculations

The quantum–chemical calculations for UV–vis transitions in aqueous solution of H₃AD, H₂ATN and H₃ATD in hydrazone and azo forms were done with the Gaussian09 suite. The calculations were performed using time dependent density functional theory (TD–DFT) which could provide a reliable description of electronic excited states of molecular systems.²⁸ Two different hybrid functionals have been used: B3LYP and mPW1PW91 that have been shown to be promising in previous benchmarks.^{28–32} The same basis set of 6–311++G(d,p) was used for the two hybrid functionals as it yielded nearly perfectly converged results for most parameters of interest.²⁹ All the ground state geometry structures except the hydrazone form of H₂ATN were optimized using B3LYP functional with 6–311++G(d,p) basis set, so to avoid that the quality of the geometry interferes with the evaluation of the performances of the functionals for transition energies.³⁰ The structure of H₂ATN in hydrazone form was based on the crystal structure obtained in this work.

2.4. Syntheses of H₃AD, H₂ATN and H₃ATD

The preparation of H₃AD, H₂ATN and H₃ATD can be readily achieved by a two-step reaction, according to the report method in reference 35. 3 mL concentrated hydrochloric acid was added to 0.02 mol 3-amino-1,2,4-triazole (1.68 g) or 0.02 mol 5-amino-tetrazole (1.70 g) in 15 mL water. The mixture solution was cooled in an ice bath keeping temperature around 0–5°C and diazotized by addition of 0.02 mol NaNO₂

(1.38 g) in 10 mL water and stirred for 30 min. Then a solution of 2,7-dihydroxynaphthalene (0.02 mol, 3.2 g) or 2-naphthol (0.02 mol, 2.88 g) in 30 mL ethanol was slowly added to the above mixture solution (Scheme 1). The resulting mixture was stirred for 12 h at room temperature and a red precipitate of H₃AD, orange precipitate of H₂ATN and crimson precipitate of H₃ATD were obtained. The red crystals of H₃AD were obtained via diffusion method by dissolving crude product of H₃AD in N,N-dimethylformamide (DMF) and using water as diffusion layer. The crude product of H₂ATN recrystallized in ethanol and orange crystals suitable for X-ray single crystal structural analyses were obtained. The crimson crystals of H₃ATD were obtained via diffusion method by dissolving crude product of H₃ATD in DMF and using isopropanol as diffusion layer. Anal. Calcd for H₃AD of C₁₂H₉N₅O₂: C, 56.47; H, 3.53; N, 27.45%; found: C, 56.32; H, 3.66; N, 27.56%; IR (KBr): 2953, 1606, 1507, 1450, 1401, 1324, 1256, 1216, 1181, 1136, 1099, 1064, 1041, 981, 840, 761, 677, 562, 511, 424 cm⁻¹; ¹H NMR (500 MHz, DMSO): δ (ppm) 15.70 (s, 1H), 14.36 (s, 1H), 10.21 (s, 1H), 8.69 (s, 1H), 7.87 (d, $J = 9.4$ Hz, 2H), 7.63 (d, $J = 8.5$ Hz, 1H), 6.95 (d, $J = 7.7$ Hz, 1H), 6.66 (d, $J = 9.3$ Hz, 1H); MS: m/z (%): 254.1 [M–H]⁻. Anal. Calcd for H₂ATN of C₁₁H₈N₆O: C, 55.00; H, 3.33; N, 35.00%; found: C, 55.12; H, 3.41; N, 35.13%; IR (KBr): 2932, 1655, 1603, 1507, 1411, 1324, 1256, 1227, 1192, 1141, 1102, 1079, 1054, 837, 707, 665, 558, 508, 447, 417 cm⁻¹; ¹H NMR (500 MHz, DMSO): δ (ppm) 15.17 (s, 1H), 8.60 (d, $J = 8.1$ Hz, 1H), 8.03 (d, $J = 9.6$ Hz, 1H), 7.77 (d, $J = 7.7$ Hz, 1H), 7.68–7.64 (m, 1H), 7.54 (td, $J = 7.6$ Hz and 1.2 Hz, 1H), 6.81 (d, $J = 9.6$ Hz, 1H); MS: m/z (%): 239.1 [M–H]⁻. Anal. Calcd for H₃ATD of C₁₁H₈N₆O₂: C, 51.56; H, 3.12; N, 32.81%; found: C, 51.63; H, 3.19; N, 32.89%; IR (KBr): 3105, 1614, 1542, 1480, 1410, 1324, 1256, 1219, 1143, 974, 878, 838, 737, 625, 512, 449 cm⁻¹; ¹H NMR (500 MHz, DMSO): δ (ppm) 15.03 (s, 1H), 10.30 (s, 1H), 8.02 (s, 1H), 7.91 (d, $J = 9.4$ Hz, 1H), 7.60 (d, $J = 8.5$ Hz, 1H), 6.99 (dd, $J = 8.5$ Hz and 2.5 Hz, 1H), 6.59 (d, $J = 9.4$ Hz, 1H); MS: m/z (%): 255.1 [M–H]⁻.



Scheme 1 Syntheses of H₃AD, H₂ATN, H₃ATD: (a) NaNO₂, HCl, 0–5°C, stirring; (b) 2,7-dihydroxynaphthalene or 2-naphthol, stirring at room temperature.

2.5 Synthesis of [Ni(H₂AD)₂] \cdot 4H₂O

2.5 mL aqueous solution of Ni(NO₃)₂ \cdot 6H₂O (0.1 mmol, 0.0291 g) was added slowly to a solution of H₃AD (0.2 mmol, 0.0510 g) in ethanol (17.5 mL) and stirred for 4 hours. The resulting mixture was filtered and brown block crystals of [Ni(H₂AD)₂] \cdot 4H₂O were obtained by slow evaporation of the

Table 1 The bond lengths [Å] and angles [°] for H₂ATN, [Ni(H₂AD)₂]-4H₂O and ring-closure product of H₂AD

H ₂ ATN							
Bond	Length(Å)	Bond	Length(Å)	Bond	Length(Å)	Bond	Length(Å)
N1–C2	1.3060(18)	N1–N2	1.3341(16)	C2–C3	1.4615(19)	C2–C1	1.478(2)
C3–C4	1.392(2)	C3–C8	1.402(2)	N2–C11	1.3574(19)	N3–C11	1.3257(18)
N3–N4	1.3473(17)	C8–C7	1.389(2)	C8–C9	1.441(2)	C11–N6	1.3130(18)
C1–O1	1.2401(17)	C1–C10	1.434(2)	C7–C6	1.368(2)	C10–N9	1.329(2)
N6–N5	1.3565(19)	C4–C5	1.375(2)	C5–C6	1.384(2)	N4–N5	1.2857(18)
Angle (°)		Angle (°)		Angle (°)		Angle (°)	
C2–N1–N2	118.97(12)	N1–C1–C3	116.54(13)	N1–C2–C1	123.94(13)	C3–C2–C1	119.52(13)
C4–C3–C8	118.78(14)	C4–C3–C2	122.07(14)	C8–C3–C2	119.13(13)	N1–N2–C11	117.22(13)
C11–N3–N4	108.38(13)	C7–C8–C3	119.49(14)	C7–C8–C9	121.35(15)	C3–C8–C9	119.16(14)
N6–C11–N3	109.62(14)	C6–N11–N2	124.76(14)	N3–C11–N2	125.58(14)	O1–C1–C10	121.48(14)
O1–C1–C2	121.30(14)	C10–C1–C2	117.23(14)	C6–C7–C8	121.01(16)	C9–C10–C1	121.73(15)
C11–N6–N5	104.39(12)	C5–C4–C3	120.74(15)	C10–C9–C8	123.21(15)	C4–C5–C6	120.25(16)
C7–C6–C5	119.74(15)	N5–N4–N3	105.51(13)	N4–N5–N6	112.09(12)		
[Ni(H ₂ AD) ₂]-4H ₂ O							
Bond	Length(Å)	Bond	Length(Å)	Bond	Length(Å)	Bond	Length(Å)
Ni1–Ni1 ¹	2.029(3)	Ni1–N1	2.029(3)	Ni1–O1 ¹	2.043(3)	Ni1–O1	2.043(3)
Ni1–N3	2.066(4)	Ni1–N3 ¹	2.066(4)	N1–N2	1.302(5)	N1–C1	1.341(5)
N2–C11	1.372(6)	N3–N4	1.325(6)	N3–C11	1.370(6)	N4–C12	1.303(7)
N5–C11	1.317(6)	N5–C12	1.341(6)	O1–C2	1.288(5)	O2–C8	1.360(5)
C1–C2	1.423(5)	C1–C10	1.469(5)	C2–C3	1.423(6)	C3–C4	1.350(6)
C4–C5	1.415(6)	C5–C6	1.403(6)	C5–C10	1.410(6)	C6–C7	1.361(6)
C7–C8	1.386(6)	C8–C9	1.386(5)	C9–C10	1.396(5)		
Angle (°)		Angle (°)		Angle (°)		Angle (°)	
Ni1 ¹ –Ni1–N1	176.49(19)	Ni1 ¹ –Ni1–O1	98.38(12)	N1–Ni1–O1	79.08(12)	Ni1 ¹ –Ni1–O1 ¹	79.08(12)
N1–Ni1–O1 ¹	98.38(12)	O1–Ni1–O1 ¹	88.71(19)	N1 ¹ –Ni1–N3	104.79(14)	N1–Ni1–N3	77.69(14)
O1–Ni1–N3	156.74(13)	O1 ¹ –Ni1–N3	93.63(15)	N1 ¹ –Ni1–N3 ¹	77.69(14)	N1–Ni1–N3 ¹	104.79(14)
O1–Ni1–N3 ¹	93.63(15)	O1 ¹ –Ni1–N3 ¹	156.74(13)	N3–Ni1–N3 ¹	93.3(2)	N2–N1–C1	123.5(3)
N2–N1–Ni1	120.6(3)	C1–N1–Ni1	115.9(3)	N1–N2–C11	109.0(3)	N4–N3–C11	102.9(4)
N4–N3–Ni1	148.6(3)	C11–N3–Ni1	108.4(3)	C12–N4–N3	110.2(4)	C11–N5–C12	103.2(4)
C2–O1–Ni1	111.9(3)	N1–C1–C2	111.4(3)	N1–C1–C10	128.1(4)	C2–C1–C10	120.4(4)
O1–C2–C3	119.0(4)	O1–C2–C1	121.6(4)	C3–C2–C1	119.4(4)	C4–C3–C2	119.8(4)
C3–C4–C5	123.0(4)	C6–C5–C10	119.5(4)	C6–C5–C4	120.1(4)	C10–C5–C4	120.4(4)
C7–C6–C5	121.0(4)	C6–C7–C8	120.0(4)	O2–C8–C9	117.7(4)	O2–C8–C7	121.8(4)
C9–C8–C7	120.5(4)	C8–C9–C10	120.4(4)	C9–C10–C5	118.7(3)	C9–C10–C1	124.3(4)
C5–C10–C1	116.9(4)	N5–C11–N3	112.8(4)	N5–C11–N2	123.0(4)	N3–C11–N2	124.2(4)
N4–C12–N5	110.9(4)						
ring-closure product of H ₂ AD							
Bond	Length(Å)	Bond	Length(Å)	Bond	Length(Å)	Bond	Length(Å)
N1–N2	1.352(2)	N1–C2	1.366(3)	N1–C4	1.372(3)	N3–C2	1.323(3)
N3–C1	1.342(3)	N2–C1	1.329(3)	N4–N5	1.312(2)	N4–C2	1.350(3)
N5–C3	1.370(2)	C8–C9	1.392(3)	C8–C7	1.429(3)	C8–C3	1.437(3)
C3–C4	1.397(3)	C4–C5	1.397(3)	C9–C10	1.374(3)	C12–C11	1.351(3)
C12–C7	1.409(3)	C11–C10	1.406(3)	C6–C5	1.362(3)	C6–C7	1.407(3)
C10–O1	1.345(3)						
Angle (°)		Angle (°)		Angle (°)		Angle (°)	
N2–N1–C2	110.11(18)	N2–N1–C4	128.64(18)	C2–N1–C4	121.30(19)	C2–N3–C1	101.82(19)
C1–N2–N1	100.70(19)	N5–N4–C2	118.58(18)	N4–N5–C3	120.39(19)	C9–C8–C7	119.90(19)
C9–C8–C3	123.12(18)	C7–C8–C3	117.0(2)	N5–C3–C4	123.3(2)	N5–C3–C8	117.3(2)
C10–C9–C8	120.1(2)	C11–C12–C7	121.3(2)	C12–C11–C10	120.5(2)	C5–C6–C7	122.6(2)
C4–C3–C8	119.32(18)	N1–C4–C3	114.01(18)	N1–C4–C5	122.9(2)	C3–C4–C5	123.1(2)
O1–C10–C9	123.4(2)	O1–C10–C11	116.3(2)	C9–C10–C11	120.3(2)	C6–C7–C12	121.7(2)
C6–C7–C8	120.3(2)	C12–C7–C8	117.9(2)	N3–C2–N4	127.7(2)	N3–C2–N1	109.9(2)
N4–C2–N1	122.4(2)	C6–C5–C4	117.6(2)	N2–C1–N3	117.4(2)		

¹1-Y+X, 2-Y, 3/2-Z

filtrate after one week and washed with distilled water. Yield: 18% (based on Ni²⁺). IR (KBr): 3128, 2939, 1611, 1597, 1500, 1477, 1312, 1276, 1215, 1144, 970, 881, 842, 512 cm⁻¹.

3. Results and discussion

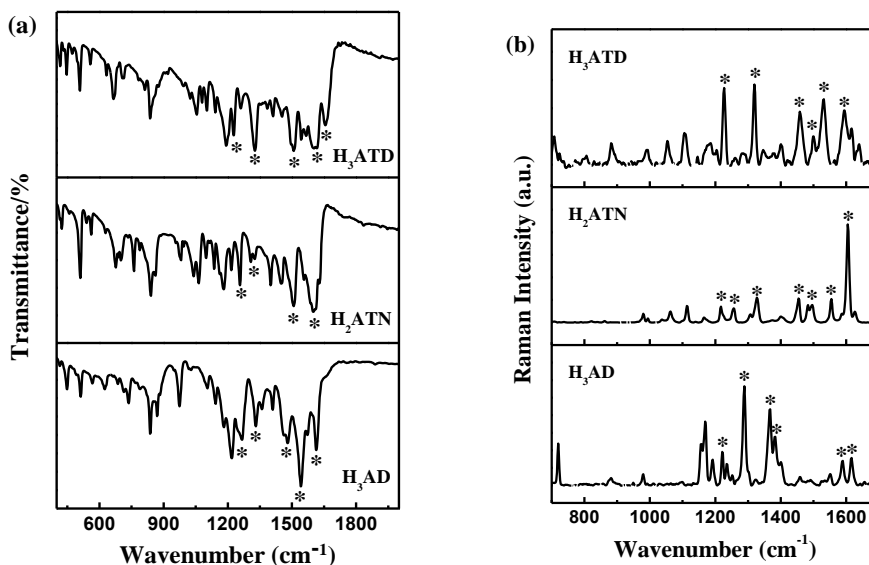


Fig. 1 (a) IR spectra for H₃AD, H₂ATN and H₃ATD, (b) Raman spectra for H₃AD, H₂ATN and H₃ATD in solid state.

The triazole/tetrazole azo dyes studied in this work were prepared by reaction of 3-amino-1,2,4-triazole or 5-amino-tetrazole with NaNO₂ in the presence of HCl at 0–5 °C and further coupling with 2,7-dihydroxynaphthalene or 2-naphthol at room temperature. The three azo dyes of H₃AD, H₂ATN and H₃ATD showed azo–hydrazone tautomerism and this property has demonstrated by IR, Raman, ¹H, ¹³C NMR spectra, UV–vis and X-ray single-crystal diffraction techniques as well as TD–DFT calculations.

3.1. IR and Raman spectroscopy analyses

The measured IR and Raman spectra for H₃AD, H₂ATN and H₃ATD are given in Fig. 1. Comparing with the azo structures, the bands in the region between 1600 and 1200 cm⁻¹ are the characteristic peaks for hydrazone structures in IR spectra.¹⁹ The bands at 1606–1659 cm⁻¹ for H₃AD, H₂ATN and H₃ATD can be assigned as δ NH, ν CC vibrations. The band located in 1507 cm⁻¹ for H₃AD, H₂ATN and H₃ATD is attributed to δ NH, ν CO, ν C=N, β CH vibrations. The bands around 1324 cm⁻¹ and 1256 cm⁻¹ for H₃AD, H₂ATN and H₃ATD are mainly assigned to δ NH, ν N–N, β CH, ν CC vibrations (Fig. 1a). All of these vibrations suggest that the hydrazone isomers are the predominant structures for H₃AD, H₂ATN and H₃ATD in solid state. The assignments of Raman spectra also support the presence of hydrazone tautomers in the solid state for three azo compounds studied. As can be seen in Fig. 1b, the bands at 1529–1615 cm⁻¹ for H₃AD, H₂ATN and H₃ATD are mainly due to δ NH, β CH, ν CC vibrations. The bands at 1496–1501 cm⁻¹ for H₃AD, H₂ATN and H₃ATD are mainly assigned as ν C=O vibrations and the bands at 1322–1386 cm⁻¹ are mainly assigned to ν CC vibrations. The bands at 1211–1288 cm⁻¹ are attributed to δ NH, ν N–N, β CH, ν CC vibrations.¹⁹

3.2. ¹H NMR and ¹³C NMR spectroscopy studies

The ¹H and ¹³C NMR spectra of H₃AD, H₂ATN and H₃ATD have been measured in DMSO–d₆ solution. As can be seen in Fig. 2b,

the chemical shifts (δ) of hydrogen atoms of naphthalene rings in H₃AD, H₂ATN and H₃ATD are located from 6.58 to 8.69 ppm, which can be easily assigned by means of the deshielding effects and the split of peaks. The active peaks appearing in low field of $\delta = 15.70$ ppm in H₃AD, $\delta = 15.17$ ppm in H₂ATN and $\delta = 15.03$ ppm in H₃ATD with integral height of 1.0 should originate from the proton of N–H group, which come from the hydrazone form and can be explained by the presence of a very strong intramolecular hydrogen bond between C=O and N–H group.⁵ The peaks located in 10.21 ppm for H₃AD and 10.30 ppm for H₃ATD should attribute to the proton of phenolic group (OH). The active peak of $\delta = 14.36$ ppm with integral height of 1.0 in H₃AD should originate from the proton of NH group, which may come from the triazole moiety. However, the proton of NH group from the tetrazole moiety in H₂ATN and H₃ATD can not be observed.

According to the literature, dyes which structures are in the azo form present a peak at about 160 ppm in the ¹³C NMR spectra, assigned to the carbon atom bonded to the hydroxyl group, while dyes which present the hydrazone form as the predominant show a peak at approximately 170 ppm in the ¹³C NMR spectra, assigned to the carbon atom from the carbonyl group.³⁶ For the compounds analyzed in this paper, the chemical shifts of C1 for H₃AD, H₂ATN and H₃ATD are 171.31 ppm, 177.12 ppm and 175.92 ppm, respectively. It seems reasonable to conclude that the hydrazone tautomers of three compounds are the predominant forms in DMSO–d₆ solution. The chemical shifts for other carbon atoms of H₃AD in DMSO–d₆ solution are 106.39 (C8), 116.68 (C6), 120.35 (C2), 122.11 (C5), 130.41 (C10), 131.55 (C4), 135.31 (C9), 141.99 (C11), 145.41 (C2), 159.44 (C12), 163.08 (C7). The chemical shifts for other carbon atoms of H₂ATN in DMSO–d₆ solution are 123.56 (C2), 125.44 (C5), 128.54 (C7), 129.16 (C10), 130.02 (C8), 130.53 (C6), 132.11 (C9), 132.74 (C4), 144.68 (C2) and 158.30 (C11). The chemical shifts for other carbon atoms of H₃ATD in

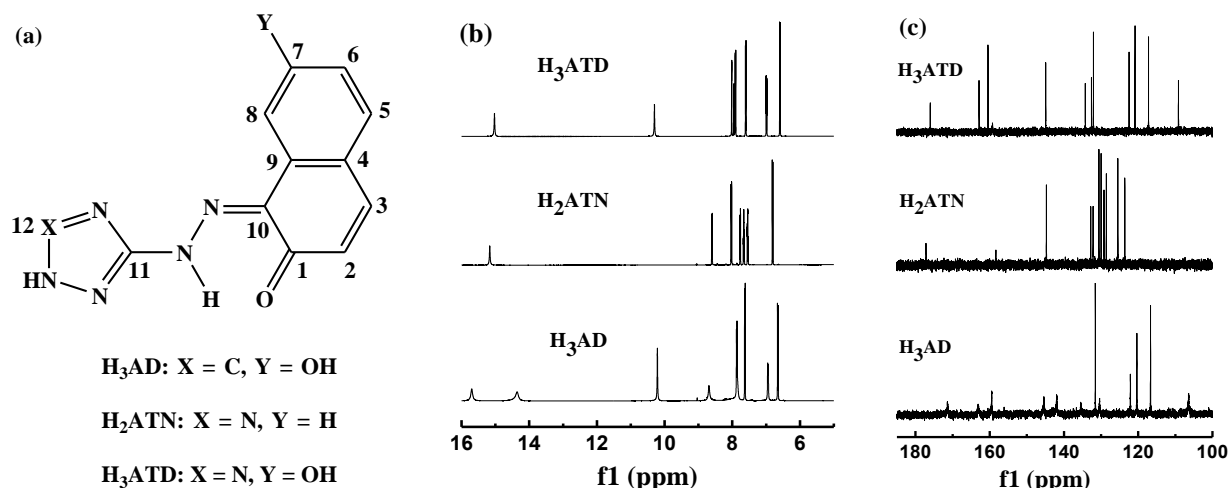


Fig. 2 (a) The C atomic labeling diagrams for H_3AD , H_2ATN and H_3ATD , (b) Schematic illustration for ^1H NMR peaks of H_3AD , H_2ATN and H_3ATD in $\text{DMSO}-d_6$, (c) Schematic illustration for ^{13}C NMR peaks of H_3AD , H_2ATN and H_3ATD in $\text{DMSO}-d_6$.

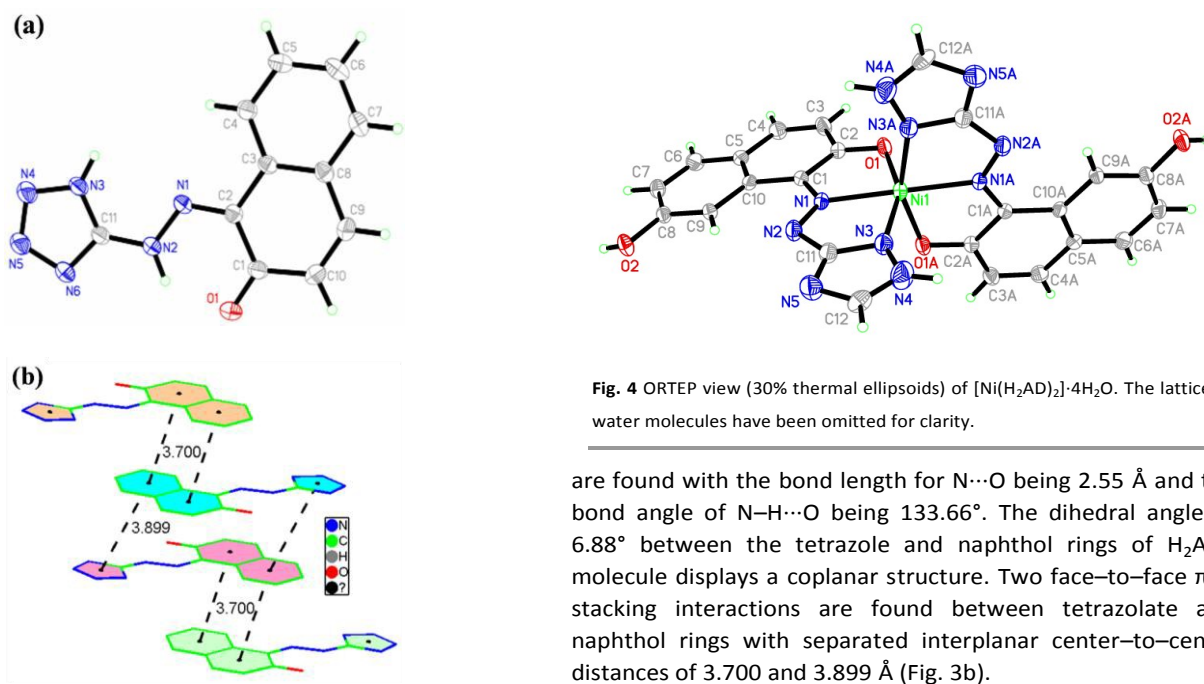


Fig. 3 (a) The atomic labeling diagram of H_2ATN , (b) The face-to-face $\pi-\pi$ stacking interactions diagram of H_2ATN .

$\text{DMSO}-d_6$ solution are 109.06 (C8), 117.13 (C6), 120.77 (C2), 122.36 (C5), 131.96 (C10), 132.48 (C4), 134.15 (C9), 144.82 (C3), 160.36 (C11), 162.77 (C7).

3.3. Crystal structures of H_2ATN and $[\text{Ni}(\text{H}_2\text{AD})_2] \cdot 4\text{H}_2\text{O}$

The atomic labeling diagram for H_2ATN is shown in Fig. 3a. Each unit cell of H_2ATN contains a fundamental H_2ATN molecule. The C1–O1 bond length is 1.2401(17) Å and the N1–N2 bond length is 1.3341(16) Å, which indicate a neutral hydrazone isomer. A N–H...O hydrogen bonding interactions

Fig. 4 ORTEP view (30% thermal ellipsoids) of $[\text{Ni}(\text{H}_2\text{AD})_2] \cdot 4\text{H}_2\text{O}$. The lattice water molecules have been omitted for clarity.

are found with the bond length for N...O being 2.55 Å and the bond angle of N–H...O being 133.66°. The dihedral angle of 6.88° between the tetrazole and naphthol rings of H_2ATN molecule displays a coplanar structure. Two face-to-face $\pi-\pi$ stacking interactions are found between tetrazolate and naphthol rings with separated interplanar center-to-center distances of 3.700 and 3.899 Å (Fig. 3b).

Single-crystal X-ray diffraction analysis reveals that compound $[\text{Ni}(\text{H}_2\text{AD})_2] \cdot 4\text{H}_2\text{O}$ crystallizes in trigonal system, $P-3c1$ space group. Each Ni^{2+} ion coordinates to two oxygen atoms and four nitrogen atoms including two azo nitrogen atoms from two anionic ligands of H_2AD^- to give a distorted octahedral geometry (Fig. 4). The axial N1–Ni–N1A bond angle is 176.65°, which slightly deviates from linearity of 180°. Each H_2AD^- anion acts as a tridentate ligand with a triazole nitrogen atom and an azo nitrogen atom as well as a hydroxyl oxygen atom coordinating to a Ni^{2+} ion. The bond length for N1–N2 is 1.294(5) Å and the bond length for C2–O1 is 1.286(4) Å, which indicate H_2AD^- anion display an azo isomer.

3.4. UV–Vis absorption of H_3AD , H_2ATN and H_3ATD

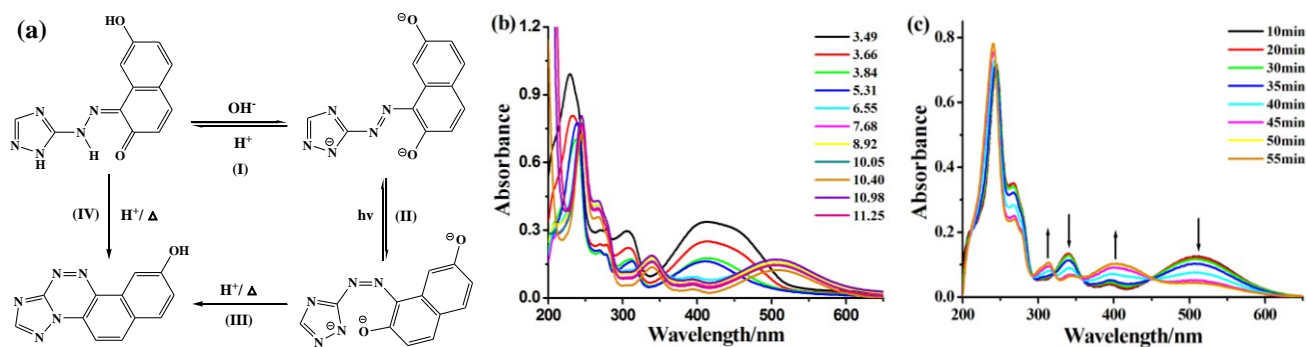


Fig. 5 (a) The pH-controllable azo-hydrazone tautomerism (I), *trans-cis* photochromism (II) and ring-closure reaction formed by acid catalyzed intramolecular dehydration and C–N bond formation reaction (III, IV) of H₃AD, (b) The pH-dependent UV–vis spectral changes for the aqueous solution of H₃AD, (c) The UV–vis spectral changes under 365 nm UV light irradiation at room temperature for the basic solutions of H₃AD with pH of 10.40.

UV–Vis spectra of H₃AD, H₂ATN and H₃ATD have been recorded in their aqueous solutions with the concentration of $1.82 \times 10^{-4} \text{ mol}\cdot\text{dm}^{-3}$, $2.22 \times 10^{-4} \text{ mol}\cdot\text{dm}^{-3}$ and $1.33 \times 10^{-4} \text{ mol}\cdot\text{dm}^{-3}$, respectively. The pH driving azo-hydrazone tautomerism experiments are carried out by adding different amounts of $2 \text{ mol}\cdot\text{dm}^{-3}$ HCl or NaOH solutions to their solutions at room temperature. As illustrated in Fig. 5b, the pH of H₃AD in aqueous solutions ($1.82 \times 10^{-4} \text{ mol}\cdot\text{dm}^{-3}$) is 5.31. For the H₃AD solution, there are three obvious absorption peaks centered at 238 nm, 313 nm and 411 nm and a weaker shoulder peak around 268 nm. The absorption peaks around 313 and 411 nm should be ascribed to the π – π^* transitions of hydrazone tautomer of H₃AD.⁴ When the pH increase from 3.49 to 5.31 by titration with $2 \text{ mol}\cdot\text{dm}^{-3}$ HCl solution, two absorption peaks at 313 and 411 nm decrease in intensity. When the pH increases from 6.55 to 11.25 by titration with $2 \text{ mol}\cdot\text{dm}^{-3}$ NaOH solution, two main absorption peaks at 313 and 411 nm disappear and two new red-shifted peaks centered at 340 and 508 nm emerge. The red-shifted absorption spectra in the alkaline condition have clearly suggested a hydrazone-azo tautomeric equilibrium and the ionization reaction in the medium (Fig. 5a). As a result, with the formation of deprotonated azo anionic species, the electron density around the chromophoric azo unit increases, which would lead to the increase in electron delocalization and result in a red shift.³⁷ It is concluded that there is a hydrazone-azo tautomeric equilibrium in solution and the ratio of the hydrazone form is dominating in acid and neutral conditions, while the azo form is dominating with the increase of pH values. Fig. 5c gives the photochromic properties for the alkaline aqueous solution of H₃AD with pH = 10.40 under 365 nm UV light irradiation at room temperature. Upon irradiation for 55 min with 365 nm UV light irradiation, the two main absorption peaks at 340 and 508 nm are continuously weakened till disappear and two new blue-shifted peaks at 313 and 400 nm are continuously enhanced in basic solutions of H₃AD. The changes of UV–vis absorption spectra for the basic solutions of H₃AD under 365 nm UV light irradiation should be attributed to the reversible *trans-enol* to *cis-enol* photochromic properties of AD³⁻ anion. Very interestingly, when the acid solution of H₃AD is heated, a yellow precipitate

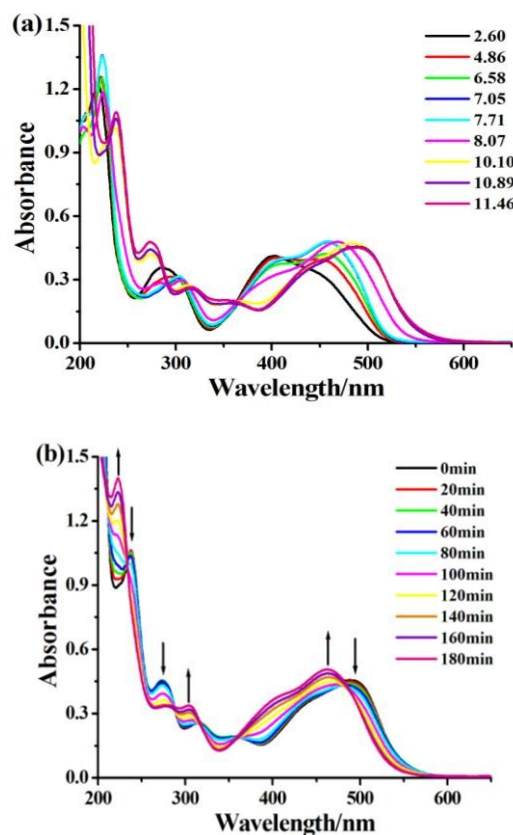


Fig. 6 (a) The pH-dependent UV–vis spectral changes for the aqueous solution of H₂ATN, (b) The UV–vis spectral changes under 365 nm UV light irradiation at room temperature for the basic solutions of H₂ATN with pH of 10.89.

with formula weight of $236 \text{ g}\cdot\text{mol}^{-1}$ was generated and its crystal was lucky obtained. This may attribute to ring-closure reaction formed by acid catalyzed intramolecular dehydration and C–N bond formation reaction of H₃AD (Fig. 5a). Fig. S1 gives the mass spectrum of the yellow precipitate and its crystal structure (ESI[†]).

In order to compare the differences before and after metal-ion complexation, UV–vis spectra of H₃AD and its mixed

solution with transition metal chlorates of Cd(II), Zn(II), Ni(II) and Co(II) ions have been recorded in their aqueous solutions with the same concentration of $1.82 \times 10^{-4} \text{ mol}\cdot\text{dm}^{-3}$, as can be seen in Fig. S2a (ESI[†]). Upon the addition of different transition metal ions of Cd(II), Zn(II), Ni(II) and Co(II), the absorption peak at 411 nm is red-shifted to 500 nm. It can be deduced that a transformation from the hydrazone to azo configuration takes place after metal-ion complexation and the anionic ligand in the complexes should be in the azo form and this has been demonstrated by the crystal structure of $[\text{Ni}(\text{H}_2\text{AN})_2]\cdot 4\text{H}_2\text{O}$.³⁶ Obviously, the neutral hydrazone of H_3AD to azo anionic configuration undergo a coordination-coupled proton transfer.

Fig. 6a gives the pH-dependent UV-vis spectral changes for the aqueous solution of H_2ATN . The pH of H_2ATN in aqueous solutions ($2.22 \times 10^{-4} \text{ mol}\cdot\text{dm}^{-3}$) is 7.05. For the H_2ATN solution, there are three obvious absorption peaks centered at 223 nm, 304 nm and 459 nm and a weaker shoulder peak around 401 nm. The absorption peaks around 223, 304, 401 nm should be ascribed to the $\pi\text{-}\pi^*$ transitions of hydrazone tautomer of H_2ATN . Additionally, the peak around 459 nm should be ascribed to the $\pi\text{-}\pi^*$ transitions between the naphthalene ring and the tetrazole ring from the neutral *trans*-azo tautomer of H_2ATN .³⁷ When the pH increase from 2.60 to 7.05 by titration with $2 \text{ mol}\cdot\text{dm}^{-3}$ HCl solution, the strength of two absorption peaks at 308 and 401 nm decrease slightly and the absorption peak at 459 nm increase tardily. When the pH increases from 7.71 to 11.46 by titration with $2 \text{ mol}\cdot\text{dm}^{-3}$ NaOH solution, the strength of two absorption peaks at 308 and 401 nm are weakened till disappear and three new peaks around 238, 274, 316 nm emerge and the peak at 459 nm redshifted to 491 nm. The four red-shifted absorption peaks at 238, 274, 316 and 491 nm in the strong basic solution and enhancement in intensity have clearly supported a hydrazone-azo tautomeric equilibrium and the ionization reaction in the medium. Consequently, with the formation of deprotonated azo anionic species, the electron density around the chromophoric azo unit increases, which would lead to the increase in electron delocalization and result in a red shift.³⁷ The shift of absorption peaks from 401 to 459 nm with the increase of pH values should be ascribed to reversible hydrazone to azo tautomerism. Fig. 6b gives the photochromic properties for the alkaline aqueous solution of H_2ATN with pH = 10.89 under 365 nm UV light irradiation at room temperature. Upon irradiation for 180 min, the three main absorption peaks at 238, 274 and 491 nm are continuously weakened till disappear and three new peaks at 223, 305 and 463 nm are continuously enhanced in basic solutions of H_2ATN . The changes of UV-vis absorption spectra for the basic solutions of H_2ATN under the 365 nm UV light irradiation should be attributed to the reversible *trans*-enol to *cis*-enol photochromic properties of ATN^{2-} anion.

The UV-vis spectra of H_2ATN and its mixed solutions with transition metal chlorates of Cd(II), Zn(II), Ni(II) and Co(II) ions with the same concentration of $2.22 \times 10^{-4} \text{ mol}\cdot\text{dm}^{-3}$ are shown in Fig. S2b (ESI[†]). The absorption peak at 401 nm disappears and the peak at 459 nm is redshifted to 470, 482, 492 and 555 nm for Cd(II), Zn(II), Ni(II) and Co(II) mixed

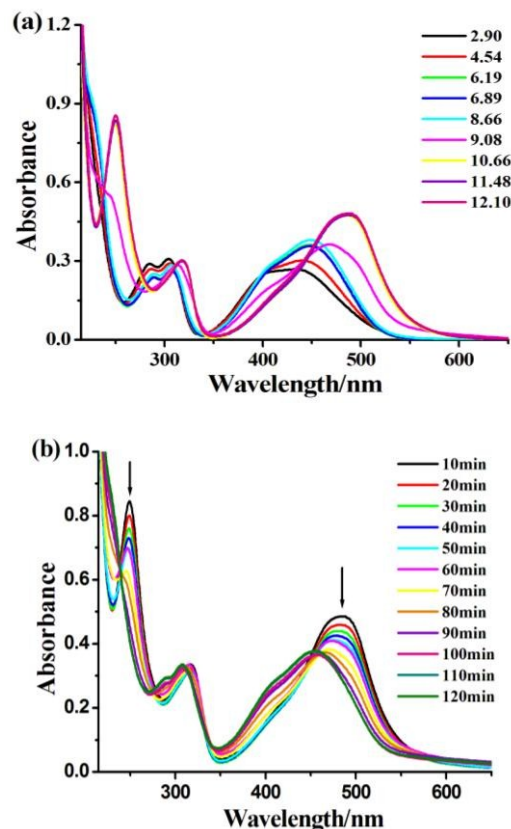


Fig. 7 (a) The pH-dependent UV-vis spectral changes for the aqueous solution of H_3ATD , (b) The UV-vis spectral changes under 365 nm UV light irradiation at room temperature for the basic solutions of H_3ATD with pH of 10.66.

solution, respectively. So it is deduced that a transformation from the hydrazone to azo configuration takes place after metal-ion complexation and the ligand in the complexes should be in the azo form.³⁸

Fig. 7a shows the pH-dependent UV-vis spectral changes for the aqueous solution of H_3ATD . The pH of H_3ATD in aqueous solutions ($1.33 \times 10^{-4} \text{ mol}\cdot\text{dm}^{-3}$) is 8.66. In order to finely adjust the pH values from 2.90 to 12.10, the H_3ATD solution has been added the aqueous solutions with $2 \text{ mol}\cdot\text{dm}^{-3}$ HCl or NaOH. The absorption peak located in 403 nm disappears as the pH value increase to 12.10 and the strength of main absorption peak around 450 nm is enhanced till pH = 8.66 then begins to red shift to 488 nm with the increase of pH values from 9.08 to 12.10. The red-shifted absorption peaks in the strong basic solution have also supported a hydrazone-azo tautomeric equilibrium and the ionization reaction in the medium. The absorption peaks around 403 nm should be ascribed to the $\pi\text{-}\pi^*$ transitions of hydrazone tautomer of H_3ATD , while the peak around 450 nm should be ascribed to the $\pi\text{-}\pi^*$ transitions between the naphthalene ring and the tetrazole ring from the neutral *trans*-azo tautomer of H_3ATD . Upon irradiation with 365 nm UV light, the main absorption peak around 250 and 485 nm for the basic aqueous solution of H_3ATD are continuously weakened and a new peak centered at

455 nm emerge (Fig. 7b). The changes of UV-vis absorption spectra for the basic solutions of H₃ATD under 365 nm UV light irradiation also attributed to the reversible *trans*-enol to *cis*-enol photochromic properties of ATD³⁻ anion. When adding the aqueous solutions with transition metal ions of Cd(II), Zn(II), Ni(II) and Co(II), the absorption peak at 450 nm red-shifted to 490 nm, which should be deduced that a transformation from the hydrazone to azo configuration takes place after metal-ion complexation (Fig. S2c, ESI[†]).

3.5. The photoluminescence of H₃AD

The fluorescence properties of H₃AD in neutral and basic ethanol solutions are studied at room temperature with the same concentration (2.43×10^{-3} mol·dm⁻³, Fig. S3, ESI[†]). In neutral ethanol solution, H₃AD displays an intense green fluorescent emission with maximum band at 574 nm upon 415 nm light excitation, which may probably be attributed to $\pi \rightarrow \pi^*$ or $n \rightarrow \pi^*$ transitions. In basic ethanol solution, H₃AD shows a weak blue-shift emission band at 472 nm under 415 nm light excitation. However, both H₂ATN and H₃ATD in neutral and basic ethanol solutions do not show any fluorescence.

3.6. TD-DFT calculation analyses

Fig. 8 gives the calculated electronic spectra for hydrazone and azo forms of H₂ATN and H₃ATD in aqueous solution. The

calculated electronic spectrum for hydrazone form of H₃AD is shown in Fig. S4 (ESI[†]). The spectra of H₃AD, H₂ATN and H₃ATD exist three calculated bands, with a red shift found in going from hydrazone to azo tautomer. For the hydrazone form of H₂ATN, the absorption peak at 213 nm involves mainly a transition from molecular orbital (MO) 61 (HOMO-1) to LUMO+3 (MO = 66) with oscillator strength $f = 0.4074$, the absorption peak at 303 nm is attributed to HOMO-3 (MO = 59) \rightarrow LUMO (MO = 63) with oscillator strength $f = 0.2060$ and the band at 404 nm is attributed to HOMO-1 (MO = 61) \rightarrow LUMO (MO = 63) with oscillator strength $f = 0.2659$, which are coincide with experimental observed bands of 223, 304 and 401 nm in acid condition. For the azo isomer of H₂ATN, the absorption peak at 224 nm is assigned as HOMO-1 (MO = 61) \rightarrow LUMO+1 (MO = 64) with oscillator strength $f = 0.9412$, the absorption peak at 308 nm is assigned as HOMO-3 (MO = 59) \rightarrow LUMO (MO = 63) with oscillator strength $f = 0.4022$ and the band at 457 nm is assigned as HOMO (MO = 62) \rightarrow LUMO (MO = 63) with oscillator strength $f = 0.3562$, which are in accordance with experimental values of 223, 304 and 459 nm in neutral or alkaline condition (Fig. 8a). The corresponding molecular orbitals for both tautomeric forms of H₂ATN are given in Fig. 8b. For the hydrazone form of H₃ATD, the absorption peak at 217 nm contains mainly a transition from

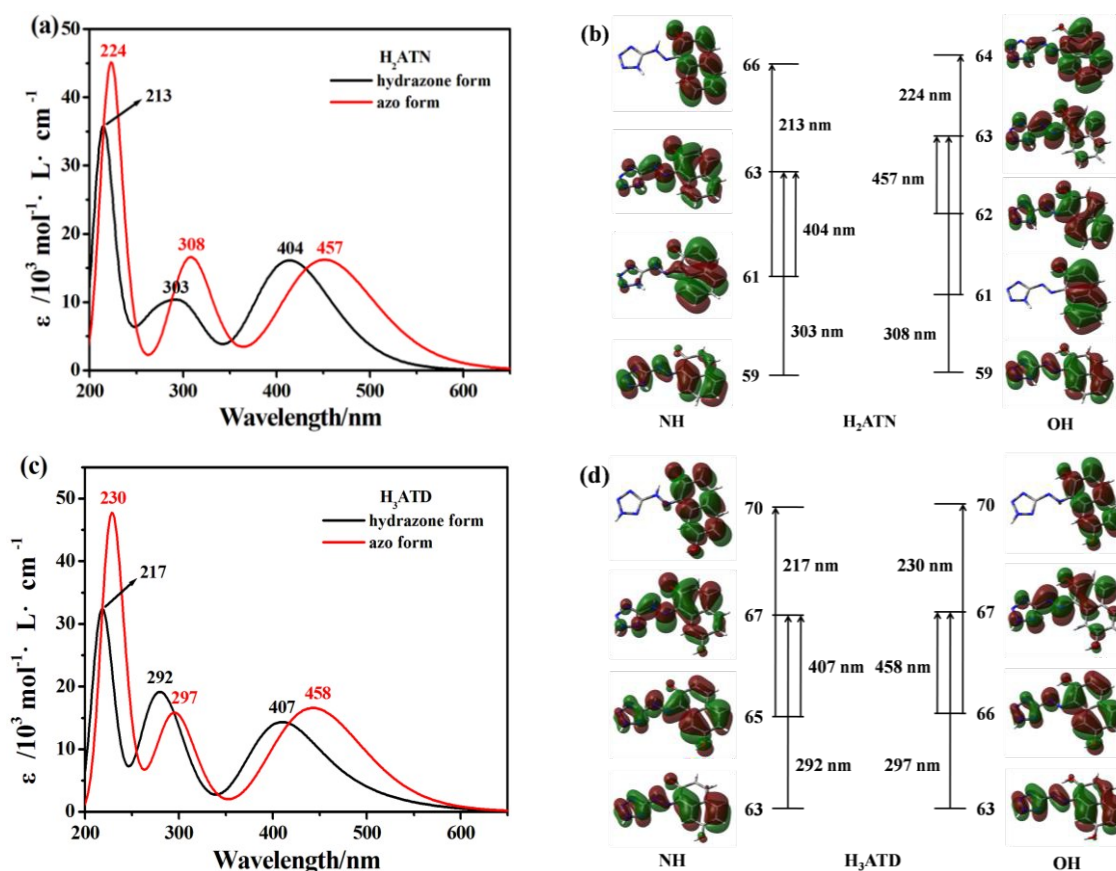


Fig. 8 (a), (c) The calculated electronic spectra of H₂ATN and H₃ATD in hydrazone and azo forms in aqueous solution, respectively, (b), (d) The molecular orbitals involved in the main electronic transitions for hydrazone and azo forms of H₂ATN and H₃ATD, respectively.

HOMO–1 (MO = 65) to LUMO+3 (MO = 70) with oscillator strength $f = 0.6913$, the absorption peak at 292 nm belongs to HOMO–3 (MO = 63) \rightarrow LUMO (MO = 67) with oscillator strength $f = 0.1821$ and the band at 407 nm belongs to HOMO–1 (MO = 65) \rightarrow LUMO (MO = 67) with oscillator strength $f = 0.3415$, which are coincide with experimental observed bands of 223, 307 and 403 nm in acid condition. For the azo isomer of H₃ATD, the absorption peak at 230 nm is assigned as HOMO (MO = 66) \rightarrow LUMO+3 (MO = 70) with oscillator strength $f = 0.6825$, the absorption peak at 297 nm is assigned as HOMO–3 (MO = 63) \rightarrow LUMO (MO = 67) with oscillator strength $f = 0.3529$ and the band at 458 nm is assigned as HOMO (MO = 66) \rightarrow LUMO (MO = 67) with oscillator strength $f = 0.2438$, which are in accordance with experimental values of 223, 307 and 450 nm in neutral or alkaline condition (Fig. 8c). The corresponding molecular orbitals for both tautomeric forms of H₃ATD are shown in Fig. 8d. For the hydrazone form of H₃AD, the absorption peak at 226 nm involves mainly a transition from molecular orbital (MO) 65 (HOMO–1) to LUMO+2 (MO = 69) with oscillator strength $f = 0.4701$, the absorption peak at 283 nm is mainly attributed to HOMO (MO = 66) \rightarrow LUMO+1 (MO = 68) with oscillator strength $f = 0.2010$ and the band at 418 nm is attributed to HOMO–1 (MO = 65) \rightarrow LUMO (MO = 67) with oscillator strength $f = 0.4394$, which are coincide with experimental observed bands of 238, 313 and 411 nm in acid condition (Fig. S4, ESI†). It is worth noting that the calculated absorption peaks for hydrazone and azo tautomers of H₃AD, H₂ATN and H₃ATD are in good accordance with the experimental ones, which further support the azo–hydrazone tautomerism in the acid and neutral or alkaline conditions in solution.

In order to validate the electronic spectra analysis for hydrazone and azo forms of H₂ATN, H₃ATD and H₃AD, another hybrid functional of mPW1PW91 has been employed, as can be seen in Fig. S5.† The calculated results using mPW1PW91 method are similar to those of B3LYP method. The gas phase electronic spectra for the three compounds using TD–DFT at B3LYP/6–311++G(d,p) level are given in Fig. S6.† The results show that the maximum absorption peaks in gas phase for the three compounds are shorter than those in aqueous solvent.

4. Conclusions

In summary, three heterocyclic azo dyes of H₃AD, H₂ATN and H₃ATD have been reported and their azo–hydrazone tautomerism have been achieved by pH control and coordination coupled proton transfer. The spectroscopic information of IR, Raman, UV–vis, ¹H, ¹³C NMR spectra and X-ray single-crystal diffraction techniques as well as TD–DFT calculations have demonstrated azo–hydrazone tautomerism in the reported three triazole/tetrazole heterocyclic azo dyes. The analysis of UV–vis spectra data have further provided a clear proof that the hydrazone form is the dominant tautomer in acidic and neutral solutions, while the azo form is the dominant one in alkaline solution. This work shows that the triazole/tetrazole heterocyclic naphthalene azo compounds are promising as potential dyes or photoswitching materials.

Acknowledgements

This work was supported by the National Natural Science Foundation of China (No. 21271052), Science and Technology Program Foundation of Guangdong (No. 2015A030313502) and Program Foundation of the second batch of innovation teams of Guangzhou Bureau of Education (13C04).

Notes and references

- 1 K. Hunger, *Industrial Dyes*, Wiley-VCH Verlag GmbH & Co.KGaA: Weinheim, FRG, 2003.
- 2 M. A. Rauf, S. Hisaindee and N. Saleh, *RSC Adv.*, 2015, **5**, 18097–18110.
- 3 L. Duarte, B. M. Giuliano, I. Reva and R. Fausto, *J Phys. Chem. A*, 2013, **117**, 10671–10680.
- 4 G. R. Ferreira, H. C. Garcia, M. R. C. Couri, H. F. D. Santos and L. F. C. de Oliveira, *J Phys. Chem. A*, 2013, **117**, 642–649.
- 5 X. C. Chen, T. Tao, Y. G. Wang, Y. X. Peng, W. Huang and H. F. Qian, *Dalton Trans.*, 2012, **41**, 11107–11115.
- 6 J. Garcia-Amorós, M. C. R. Castro, P. Coelho, M. M. M. Raposo and D. Velasco, *Chem. Commun.*, 2013, **49**, 11427–11429.
- 7 H. S. Freeman and J. C. Posey Jr, *Dyes. Pigments.*, 1992, **20**, 147–169.
- 8 S. Q. Wang, S. Y. Shen and H. J. Xu, *Dyes. Pigments.*, 2000, **44**, 195–198.
- 9 T. Wendler, C. Schütt, C. Näther and R. Herges, *J Org. Chem.*, 2012, **77**, 3284–3287.
- 10 B. L. Feringa, *Molecular Switches*, Wiley-VCH Verlag GmbH: Weinheim, FRG, 2001.
- 11 A. S. Kumar, T. Ye, T. Takami, B. C. Yu, A. K. Flatt, J. M. Tour and P. S. Weiss, *Nano. Lett.*, 2008, **8**, 1644–1648.
- 12 T. Sasaki and J. M. Tour, *Org. Lett.*, 2008, **10**, 897–900.
- 13 W. R. Browne and B. L. Feringa, *Annu. Rev. Phys. Chem.*, 2009, **60**, 407–428.
- 14 S. J. Isak, E. M. Eyring, J. D. Spikes and P. A. Meekins, *J. Photochem. Photobiol. A*, 2000, **134**, 77–85.
- 15 Y. Li, B. O. Patrick and D. Dolphin, *J Org. Chem.*, 2009, **74**, 5237–5243.
- 16 H. Y. Lee, X. L. Song, H. Park, M. H. Baik and D. Lee, *J Am. Chem. Soc.*, 2010, **132**, 12133–12144.
- 17 P. Gilli, V. Bertolasi, L. Pretto, A. Lycka and G. Gilli, *J Am. Chem. Soc.*, 2002, **124**, 13554–13567.
- 18 P. Gilli, V. Bertolasi, L. Pretto, L. Antonov and G. Gilli, *J Am. Chem. Soc.*, 2005, **127**, 4943–4953.
- 19 M. R. Almeida, R. Stephani, H. F. DosSantos and L. F. C. de Oliveira, *J Phys. Chem. A*, 2010, **114**, 526–534.
- 20 T. Aysha, A. Lycka, S. Lunák Jr., O. Machalický, M. Elsedik and R. Hrdina, *Dyes Pigments*, 2013, **98**, 547–556.
- 21 X. Su, F. R. Robbins and I. Aprahamian, *Angew. Chem., Int. Ed.*, 2011, **50**, 1841–1844.
- 22 G. Pavlovic, L. Racane, H. Cacak and V. Tralic-Kulenovic, *Dyes. Pigments.*, 2009, **83**, 354–362.
- 23 Z. Wang and Z. W. Wu, *Text. Res. J.*, 2010, **80**, 448–453.
- 24 J. M. Lin, M. Yang, Y. X. Qiu, W. B. Chen, H. Yan, F. X. Gao, Z. J. OuYang, W. Dong and T. C. Kuang, *ChemPlusChem*, 2013, **78**, 598–604.
- 25 W. B. Chen, Z. X. Li, X. W. Yu, M. Yang, Y. X. Qiu, W. Dong and Y. Q. Sun, *DaltonTrans.*, 2014, **43**, 9090–9097.
- 26 W. B. Chen, Z. X. Li, Z. J. Ouyang, W. N. Lin, L. Yang and W. Dong, *RSC Adv.*, 2014, **4**, 61104–61113.
- 27 J. M. Lin, Y. X. Qiu, W. B. Chen, M. Yang, A. J. Zhou, W. Dong, C. E. Tian, *CrystEngComm*, 2012, **14**, 2779–2786.
- 28 H. Phillips, S. H. Zheng, A. Hyla, R. Laine, T. Goodson, III, E. Geva and B. D. Dunietz, *J. Phys. Chem. A*, 2012, **116**, 1137–1145.

- 29 D. Jacquemin, A. Planchat, C. Adamo and B. Mennucci, *J. Chem. Theory Comput.*, 2012, **8**, 2359–2372.
- 30 D. Jacquemin, V. Wathelet, E. A. Perpète and C. Adamo, *J. Chem. Theory Comput.*, 2009, **5**, 2420–2435.
- 31 J. C. Sancho-García and A. J. Pérez-Jiménez, *J. Chem. Phys.*, 2009, **131**, 084108-1–084108-11.
- 32 C. Adamo and D. Jacquemin, *Chem. Soc. Rev.*, 2013, **42**, 845–856.
- 33 A. D. Becke, *J. Chem. Phys.*, 1993, **98**, 5648–5652.
- 34 T. Yanai, D. P. Tew, N. C. Handy, *Chem. Phys. Lett.*, 2004, **393**, 51–56.
- 35 I. L. Shegal, K. V. Stanovkina, N. G. Kovalenko and L. M. Shegal, *Khim. Geterotsikl. Soedin.*, 1974, **10**, 369–371.
- 36 L. C. Abbott, S. N. Batchelor, L. Jansen, J. Oakes, J. R. L. Smith and J. N. Moore, *New. J Chem.*, 2004, **28**, 815–821.
- 37 A. Misra and M. Shahid, *J Phys. Chem. C*, 2010, **114**, 16726–16739.
- 38 X. C. Chen, Y. G. Wang, T. Tao, J. Geng, W. Huang and H. F. Qian, *Dalton Trans.*, 2013, **42**, 7679–7692.

TOC

The azo–hydrazone tautomerism for three triazole/tetrazole azo dyes can be elucidated by ^1H , ^{13}C NMR and UV–vis spectra.

